

Article

Mini Glider Design and Implementation with Wing-Folding Mechanism

Ali Anil Demircali  and Huseyin Uvet * 

Mechatronics Engineering Department, Yildiz Technical University, Yildiz Mah. Barbaros Blv. Besiktas, 34349 Istanbul, Turkey; aanil@yildiz.edu.tr

* Correspondence: huvet@yildiz.edu.tr; Tel.: +90-533-385-3023

Received: 8 August 2018; Accepted: 27 August 2018; Published: 3 September 2018



Abstract: This paper describes a mini unmanned glider's design, simulation, and manufacturing with a novel wing-folding mechanism. The mini-glider is designed for CanSat competition, which has a theme of a Mars glider concept with atmosphere data acquisition. The aim is to facilitate the transportation of the glider and to land it on the destination point by following strict rules. Having a light and compact design is important since it uses power for the transmission of sensory data only. Dimensions of the glider is produced with a wingspan that is 440 mm and a length of 304 mm. The wings can be stowed in a fixed size container that has a diameter of 125 mm and a height of 310 mm. Its weight is only 144 g and it can increase up to 500 g maximum with a payload. The mechanism, which includes springs and neodymium N48 grade magnets for a wing-folding system, is capable of being ready in 98 ms for gliding after separating from its container. The mini-glider is capable of telemetering, communicating, and conducting other sensory operations autonomously during the flight.

Keywords: MAV; autonomous system; wing-folding; reconnaissance

1. Introduction

The demand is increasing for Mini-Glidern that weigh less than 1 kg, are small in size and can also communicate with each other in order to achieve desired functionality while also being reliable, having low power usage and low cost [1,2]. In aviation, there are specialized systems that are capable of conducting field surveys by carrying multiple air vehicles such as rockets and dropping them on the target locations [3–6]. For such specialized systems, reducing the weight and size while also deploying the maximum amount of payload is crucial. Accordingly, selecting the suitable materials for the glider and finding the design parameters allow multiple gliders to be transported at the same time. For this reason, different methods such as wing-folding mechanisms have been successfully applied to reduce the volume of miniature air-vehicles in the former designs [7–10].

The international CanSat competition is a design–build–launch competition. The concept is somehow identical to a typical gun-launched air-vehicle system [11]. The air-vehicles are required to meet predefined volume restrictions of a container that is built in a rocket launcher. The wing-folding structure of the air-vehicle allows it to be contained in a small volume, and thus to be placed in a protective fixed-size container [12]. Recent research and industrial works related to gun-launched drones are principally focused on foldable fixed-wing configurations [13,14]. Our goal in this work is to ensure that the wing-folding mechanism is opened quickly and reliably immediately after separating from the rocket. It must fulfill its assigned tasks successfully according to the competition regulations [15]. It is expected that the designed glider will descend from 400 m in helical orbit in around 120 s. For this purpose, the wing structure must have a fast deploying mechanism even in low air pressure and rough wind conditions and stabilize quickly.

There are many different wing models used in literature for fixed-wing aerial vehicles, and use of Eppler and National Advisory Committee for Aeronautics (NACA) type wing structures is relatively more common [8,16]. The Eppler-793 type wing structure appears to be fit for mini-gliders and speed-critical applications, where thickness, camber, and C_L/C_D (efficiency) ratio are crucial. Since the maximum t/c thickness ratio is in the 12–16% band, 2–5% camber is the best choice for desired operational speed [17]. Eppler wing structure allows easy assembly and easy folding by virtue of not being excessively cambered. The other selection criteria to choose an Eppler wing is to have more linear behavior in the desired (previously found via simulations) alpha operational range AoA (angle of attack). In order to gather information about the atmosphere, there are fixed-wing and larger-sized heavier systems [18] or measurements with different approaches [19,20] instead of foldable wing systems. As a matter of fact, in many control applications, in order to find an optimal solution for a stable glider flight, Proportional-Integral-Derivative (PID), Adaptive and Neural network are widely used. Our glider mechanism does not have any motors attached to it; therefore, the phugoid flight mode is a necessity [21].

To achieve passive mechanical control, our aim is to combine all electronic equipment such as telemetry devices, communication devices, and sensors into a small PCB (Printed Circuit Board) while maintaining a light and compact design. According to research on related topics, our glider's C_L is higher at the same mass while also being smaller [19], and the wing-folding mechanism is also faster [9]. Moreover, there are designs whose stowed configurations are better than our glider and occupy %75 less volume and %75 less width than their deployed form. However, our primary aim is not a only wing-folding mechanism; our designed glider, which is able to land in a controlled manner via phugoid mode, can also collect data during its descent. For different approaches in literature, although the same mechanical equipment is used, we can see that sensor data retrieval experiences mishaps during the launch process [8,9]. With this method, the amount of energy needed will be kept at a minimum, resulting in a light and compact structure. There are different autonomous studies that perform sudden dive to the target point [22]. It is observed that the success at higher wind speeds (>3 m/s) and the pitch error (avg 33.29°) are considerably high, although diving with an average error of 1 m to the desired point is carried out with low altitude release (30–40 m). Although it can dive to the target point from a lower altitude than our study, autonomous separation and wing-folding mechanism have been not mentioned. In addition, despite having an open loop controller, the pitch error is quite high. There are also works related to the folding of the wings [23]. Wing deploying and folding times, efficiency and stress analyses are not given and no real test results are available.

This work is a mini-glider that can be autonomously separated at a certain height and autonomously open its wings. To the best of our knowledge, the speed optimization of the wing-unfolding and mechanical analysis regarding its unfolding speed have never been studied. Moreover, as a contribution to literature, passive glider design and implementation under certain limitations are given with application details. What should be considered in a lightweight (<1 kg) of a glider and firm foldable structure of wings are reported. Such a work, which has a mechatronics approach, can influence other works done in miniature level in future. It is worth mentioning that this mini-glider design is not just for a competition, but also for use in the other areas by further improving the design. Some possible areas in which the designed can be implemented into are as follows: transportation of medical and surgery supplies, exploration of chemical and radioactive areas, search and rescue operations, communication systems, and agriculture. With its lightweight design and low power consumption, the glider can obtain relevant flight data from all sensors. Thus, aerodynamically, a more successful design has been made.

In our work, six-degree-of-freedom movement systems were first created and simulated in MATLAB/Simulink® (version R2015a, MathWorks Inc., Natick, MA, USA) Mechanical design and the analysis of the planer is made in the 3D Solidworks® (version 2015, Dassault Systèmes, Vélizy-Villacoublay, France) program. Electronic card design is made through the Proteus® (version 7.6, Labcenter Electronics Ltd., North Yorkshire, UK) program. While the ground station

software required for communication structure is completed with Labview[®] and C# language, the microprocessor structure of the planner is made with Arduino IDE (version 1.6, Ivrea, Italy). In the second part of the work, measurement models used with satellite kinematic and dynamic equations are presented. In the third part, after the system analysis is made by COMSOL[®] (version 5.3, COMSOL Inc., Stockholm, Sweden) and the simulated studies, the fourth and last, the result section is discussed and evaluated.

2. Mathematical Model

In this section, wing design of the glider with respect to limited container size, pre-designing design parameters and their effects, and glider's dynamic properties are expressed according to operational schematic of the glider with theoretical calculations. First of all, the trajectory and working space of the glider are important design parameters to be determined since the glider dimensions, the materials used, and the desired lift force and speed are highly correlated. The basic principles of a hovering flight is demonstrated with a MATLAB[®] simulation after autonomous separation of the glider from the container [24,25]. The glider should hover along a maximum of 1000 m helical path and the duration should be as close to 120 s as possible [15]. Operational schematic can be illustrated in Figure 1. In this figure, the glider is launched to the sky by a rocket from the ground. After the autonomous separation of the rocket, the glider transmits the telemetry data which should be received by the ground station autonomously during the descent.

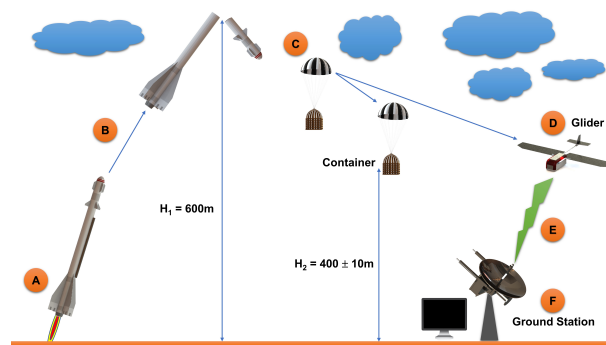


Figure 1. Glider is launched from point A and after following the trajectory B, it is separated from capsule at point C, which is 600 m above the ground. The glider has to be separated autonomously at 400 m altitude at point D and the collected data during glide have to be observed by a ground station at point F. Point E shows the data communication between a glider and the ground station.

2.1. Wing Design

The glider is designed in accordance with the rules that are given by [15]. The glider's longitudinal length and wingspan of folding position are limited by the fixed container size. For this reason, the dimensions of folding and deploying configurations are important criteria to be considered firstly. Depending on these, the weight of the glider, the position of the center of gravity, the appropriate dimensions of the glider's body and wing, and the material to be used, etc. will be determined. Pre-designed model and container including the materials and dimensions are shown in Figure 2. In this figure, dimensions of the glider are shown in the folded condition. Body and wing dimension, the position of center of gravity can also be seen. Generally, the center of gravity is adjusted to correspond to the mean aerodynamic chord (MAC) of 25% with reference to the leading edge. This position affects the performance of the glider's pitching stability when it is positioned ahead or behind. The most forward position that can be selected depends on the lift force capacity that the horizontal stabilizer can apply downwards. This force must match the pitching moment generated by the wings of the glider. Therefore, it is preferable to adjust 1/3 to the leading edge (Figure 2A,B). In the folded case of the glider, the dimensions of the container to be placed in and the material to be

produced are included (Figure 2C). Since the weight and strength are important criteria, it has been preferred to use Kevlar in the container body. Properties of both configuration of the glider can be also seen in Table 1.

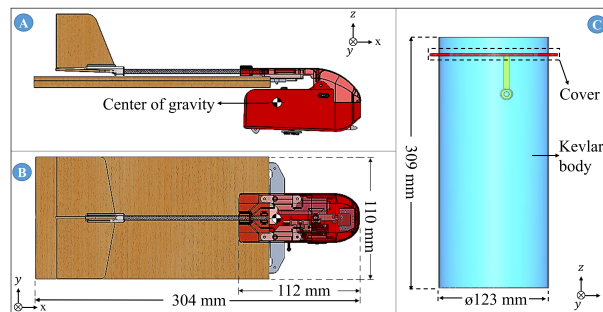


Figure 2. (A) shows the front view of the glider; (B) shows the top view of the glider with dimensions; (C) represents the fixed size container where the glider to be placed. There is a hole that is attached to the stick, which is connected to the cover, and is going to be used by the separation mechanism.

Table 1. Glider dimensions are given for folded and deployed configurations.

Configurations	Dimensions (cm)	Area (cm ²)	Volume (cm ³)
Folded	44 × 30.4 × 11	13.376	14,713.6
Deployed	11 × 30.4 × 11	334.4	3678.4

In order to determine the dynamic behaviour of the glider during descent, the required lift coefficient $C_{L,r}$ must be calculated according to the maximum pre-designed glider’s established mass. In addition, the lift force of the glider should be observed under glide condition together with the drag coefficient, C_D , that is acting on it. Lift and drag forces acting on the glider during descent will be determined by calculating these coefficients. According to pre-designed model, the mass of the container and glider, by using Kevlar material, are calculated to be 248 g and 252 g, respectively. When the glider performs a hovering movement around a helical orbit, the profile drag coefficient, $C_{D,0}$, is used to determine the calculating maximum glide speed, V_{max} (m/s). Then, aerodynamics coefficients can be determined by using angle of attack (AoA) where the range is selected from $\alpha = -9.5^\circ$ to 9.5° . In this range, $(C_L/C_D-\alpha)$ represents the lift coefficient C_L as a variable of the AoA angle, which is selected from 2° to 6° to have maximum C_L . In addition, similar stability effects can be seen in pitching moment-AoA, $(C_M-\alpha)$, for the same range of α . By using a $(C_L-\alpha)$ graph, having a more stable and reliable flight can be observed when $\alpha = 5.5^\circ$ is selected. Minimum profile drag, $C_{D,0} = 0.07$ and aspect ratio(AR), $AR = 9.466$ are determined at the same α . To determine necessary initial parameters, which need to be calculated to determine the glider dynamic behavior, Equations (1)–(5) can be used

$$V_t = \sqrt{\frac{2W}{\rho\pi C_D R^2 \cos^2(\frac{r}{2R})}} \tag{1}$$

$$V_{max} = \sqrt{\frac{2W}{\rho S} \sqrt{\frac{K}{C_{D,0}}}} \tag{2}$$

$$C_L = \frac{2L}{\rho S V^2} \tag{3}$$

$$K = \frac{1}{\pi A R e_0}, \tag{4}$$

$$Re = \frac{\rho V \bar{c}}{\mu}, \tag{5}$$

where total mass W (N), air density ρ (kg/m^3), hovering speed container, V_c and with payload V_t (m/s), total wing area $S = 0.0205$ (m^2), outer diameter of parachute R (m), inner diameter of parachute r (m), drag force D (N) [26]. In that case, $V_t, V_c, V_{max}, C_{L,r}, \alpha$ can be calculated and shown in Table 2, respectively.

Table 2. Determination of the initial necessary parameters for dynamic behavior of the glider.

Parameters	Value	Unit
V_t	8.2	(m/s)
V_c	6.1	(m/s)
V_{max}	12.5	(m/s)
$C_{L,r}$	0.4855	-
α	5.5	(°)

The lift force of the glider, which will determine maximum payload capacity for stable flight, can only be solved by determining $C_{L,r}$. By using V_t and V_c , hovering speed and duration of glide from separation from container to landing, could be expressed. V_{max} represents the maximum speed when lifting force is also at a maximum at $\alpha = 5.5^\circ$.

2.2. The Dynamic Model of the Glider

The primary goal of previous calculations is to determine dynamic behaviour of the glider. To obtain the simulation of the system, a mathematical model has to be derived by Newton motion laws with six degrees of freedom (DOF) which is illustrated in Figure 3 [27]. Nonlinear equations could yield

$$X - mg \sin(\theta) = m(\dot{U} + QW - RV), \tag{6}$$

$$Y + mg \cos(\theta) \sin(\phi) = m(\dot{V} + RU - PW), \tag{7}$$

$$Z + mg \cos(\theta) \cos(\phi) = m(\dot{W} + PV - QU), \tag{8}$$

where glider mass m (kg), aerodynamic forces X, Y, Z along body x_b, y_b, z_b -axis, respectively, axial speeds U, V, W (m/s), axial acceleration $\dot{U}, \dot{V}, \dot{W}$ (m/s^2), and angular speeds P, Q, R (rad/s). Axial acceleration can be expressed as Equations (9)–(11) and angular speeds can be calculated as Equations (12)–(14) where rolling moment L , pitching moment M , yawing moment N . Axial acceleration and angular speeds are expressed,

$$\dot{U} = RV - QW - g \sin(\theta) + X/m, \tag{9}$$

$$\dot{V} = PW - RU + g \cos(\theta) \sin(\phi) + Y/m, \tag{10}$$

$$\dot{W} = QU - PV + g \cos(\theta) \cos(\phi) + Z/m, \tag{11}$$

$$\dot{P} = (c_1R + c_2P)Q + c_3L + c_4N, \tag{12}$$

$$\dot{Q} = c_5PR - c_6(P^2 - R^2) + c_7M, \tag{13}$$

$$\dot{R} = (c_8P - c_2R)Q + c_4L + c_9N, \tag{14}$$

where

$$I = \begin{bmatrix} c_1 & c_2 & c_3 \\ c_4 & c_5 & c_6 \\ c_7 & c_8 & c_9 \end{bmatrix}. \tag{15}$$

$I \in \mathbb{R}^{3 \times 3}$ represents the moment of inertia of the glider (kgm^2) [28]. By using Equations (9)–(14), glider stability analysis is done. Solving Equations (9)–(14) yields Euler angle’s derivatives in (16)–(18). Euler angles are significant to describe since orientation of a rigid body on the fixed coordinate system could be expressed as

$$\dot{\phi} = P + \tan(\theta)(Q \sin(\phi) + R \cos(\phi)), \tag{16}$$

$$\dot{\theta} = Q \cos(\phi) - R \sin(\phi), \tag{17}$$

$$\dot{\psi} = \frac{Q \sin(\phi) + R \cos(\phi)}{\cos(\theta)}, \tag{18}$$

where $\dot{\phi}$, $\dot{\theta}$, $\dot{\psi}$. By specifying Euler angles, the resulting specific instant speed of the glider can be obtained, which is defined on the body axis. Then, the Equations (19)–(21) could be expressed including axial velocity,

$$\dot{x} = U (c\phi c\theta) + V (s\phi s\theta c\psi - c\phi s\psi) + W (c\phi s\theta c\psi + s\phi s\psi), \tag{19}$$

$$\dot{y} = U (s\phi c\theta) + V (s\phi s\theta s\psi + c\phi c\psi) + W (c\phi s\theta s\psi - s\phi c\psi), \tag{20}$$

$$\dot{z} = -U (s\theta) + V (s\phi c\psi) + W (c\phi c\theta), \tag{21}$$

where $\cos = c$, $\sin = s$. A method of evaluating the glider’s positions on the airframe is to calculate the glide duration.

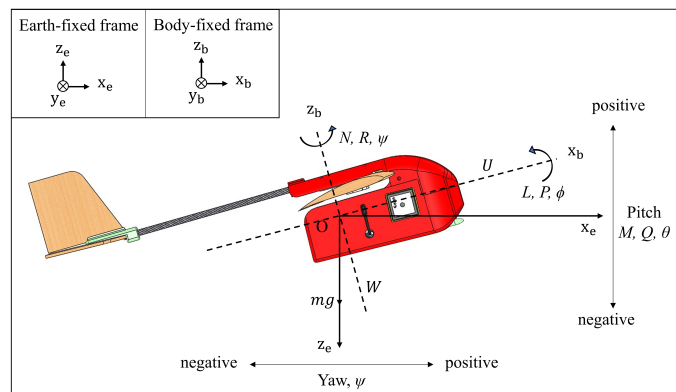


Figure 3. The center of gravity of the glider is indicated by “O” and it is given by the front view. The parameters in Equations (6)–(8) are expressed according to earth-fixed frame and body-fixed frame. Using the relationship of these frames, nonlinear equations can be derived.

2.3. Aerodynamic Calculations

The aerodynamic force coefficients need to be determined in order to perform necessary calculations when the glider is hovering in a helical orbit. To determine these coefficients, the Vortex lattice method, (VLM), is used which is a numerical method used in computational fluid dynamics. For this purpose, XFLR5[®] aerodynamic analysis is used to determine the position of the glider on the x -, y -, and z -axes after the instant speed of the glider is obtained in Section 2.2 To determine position of the glider, stability and control coefficients have to be calculated. Equation of coefficients are shown in (22)–(29):

$$c_L = c_{L,0} + c_{L,\alpha}, \tag{22}$$

$$c_D = c_{D,0} + kc_L^2, \tag{23}$$

$$c_x = -c_D c(\alpha) + c_L s(\alpha), \tag{24}$$

$$c_y = -c_{y,\beta}\beta + c_{y,p}P\left(\frac{b}{2V}\right) + c_{y,r}R\left(\frac{b}{2V}\right) + c_{y,\delta_a}\delta_a + c_{y,\delta_r}\delta_r, \tag{25}$$

$$c_z = -c_L c(\alpha) - c_D s(\alpha) - c_{L,q}Q\left(\frac{c}{2V}\right) - c_{L,\delta_e}\delta_e, \tag{26}$$

$$c_l = c_{l,\beta}\beta + c_{l,p}P\left(\frac{b}{2V}\right) + c_{l,r}R\left(\frac{b}{2V}\right) + c_{l,\delta_a}\delta_a + c_{l,\delta_r}\delta_r, \tag{27}$$

$$c_m = c_{m,0} + c_{m,\alpha}\alpha + c_{m,q}Q\left(\frac{c}{2V}\right) + c_{m,\delta_e}\delta_e, \tag{28}$$

$$c_n = c_{n,\beta}\beta + c_{n,p}P\left(\frac{b}{2V}\right) + c_{n,r}R\left(\frac{b}{2V}\right) + c_{n,\delta_a}\delta_a + c_{n,\delta_r}\delta_r, \tag{29}$$

nonlinearly with flow angles (α, β) , control surface deflections $(\delta_e, \delta_a, \delta_r)$, chord length c , wingspan b , x direction c_x , y direction c_y , z direction c_z , rolling moment c_l , pitching moment c_m , yawing moment c_n [27]. The obtained coefficients are used to calculate X, Y, Z, L, M, N [29]. Therefore, coefficients, which will be used for aerodynamic forces and moments acting on glider, are shown in Table 3.

Table 3. Aerodynamic force coefficients.

Longitudinal	Lateral
$c_{L,\alpha} = 4.8878$	$c_{y,\beta} = -0.36561$
$c_{L,q} = 8.6232$	$c_{n,\beta} = 0.09735$
$c_{D,0} = 0.07$	$c_{l,\beta} = -0.17966$
$c_D = 0.1065$	$c_{l,\beta} = -0.17966$
$c_{m,\alpha} = -3.0688$	$c_{y,r} = 0.3857$
$c_{m,q} = -20.781$	$c_{n,r} = -0.12476$
	$c_{l,r} = -0.22072$
	$c_{y,p} = -0.30632$
	$c_{n,p} = -0.10115$
	$c_{l,p} = -0.58491$

According to these coefficients, axial speeds and moments can be expanded into a set of six equations that could be used to determine X, Y, Z, L, M, N in Equations (30)–(35):

$$X = c_x q S, \tag{30}$$

$$Y = c_y q S, \tag{31}$$

$$Z = c_z q S, \tag{32}$$

$$L = c_l q S, \tag{33}$$

$$M = c_m q S c, \tag{34}$$

$$N = c_n q S b, \tag{35}$$

where dynamic pressure constant is q and wing area is S . The resultant model with the equipment is shown in Figure 4. In this figure, the communication & GPS unit provides the glider position, the camera unit is responsible for capturing images when the glider is launched (inside of the rocket), after first separation (inside of container) and after separation of the container. Lastly, the pitot tube and pressure sensor measure appropriate flight data.

Sensors collect the necessary information, and the data are recorded on an Secure Digital (SD) card and also transmitted to the ground station during glide. The battery is used to provide the necessary energy. Equipment is modelled especially so that the center of gravity is placed at the wing’s leading edge (1/3) in the glider.

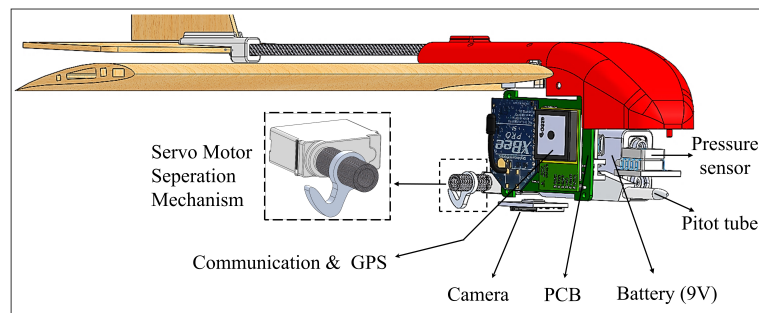


Figure 4. The model is designed by 3D Solidworks® and is shown from an isometric view including equipment. The servo motor mechanism is used to separate the glider from the container autonomously at a height of 400 m. The servo motor rotates and releases the glider at certain pre-defined height, which is measured by GPS unit.

3. Simulation and Analysis

In this section, simulation studies are described for the glider whose design is completed according to the rules and theoretical calculations based on the developed mathematical model. According to the parameters that are determined by theoretical calculations, the dynamic behavior of the glider is repeated in the simulation environment. The analysis should be performed by using authentic equipment with their properties to see more realistic behaviour in the design model to further improve the glider design after simulation. The location of center of gravity, horizontal and vertical stabilizers' size estimation, determining α to provide maximum lift, and so forth are obtained in the previous section. The simulation's aim is to compare parametric verification of the results with the theoretical calculations. Firstly, there are five different natural modes to determine stability of an aircraft which are related with two longitudinal and three lateral axes should be investigated. They are phugoid mode and short period mode for longitudinal and the spiral mode, the roll damping mode and the dutch roll mode for the lateral axis. Short period mode eigenvalues are $s_{1,2} = -15.2 \pm 5.7i$ and phugoid mode eigenvalues are $s_{3,4} = -0.1 \pm 0.2i$. All the roots are on the negative side of the Alpha axis. In this case, it represents that all the roots of the system are stable. For the roots with smaller values of the imaginary axis (beta), the damping ratio is lower. In such a case of phugoid oscillations, the change between kinetic energy (speed) and potential energy (height) is very slow, so that the glider can return to its horizontal flight position again. Phugoid mode response can be given in the form (Equation (36)) for $\sigma = \zeta\omega_n$ and $\omega = \omega_n\sqrt{1 - \zeta^2}$,

$$\lambda = \sigma + \omega i, \quad (36)$$

where damping ratio is ζ and natural frequency is ω_n . In the case of phugoid mode, the glider dynamic response according to the step input is $\lambda = -0.0392 + 1.1644i$ and $f = 0.185$ Hz. Stability and control coefficients are determined and showed that the glider can fly steadily depending on the eigenvalues.

In addition, to obtain aerodynamic behaviour of the system, XFLR5® is preferred since it has a more realistic approach through using VLM. To determine aerodynamic coefficients and efficiency, the range is selected from $\alpha = -5^\circ$ to 15° and $Re = 5 \times 10^4$ to 12.6×10^4 in Figure 5. In this figure, the pressure points on the glider's wing can be seen with an orange-red colour. The pressure coefficient c_p varies between 0.66–1.11, which determines stability and axial moments, and it is more likely to be on the leading edge. Lift coefficient $C_L = 0.66$, which is greater than $C_{L,r} = 0.4855$, which is mentioned in Section 2.1. Table 2 is found when the speed of glider is $V_{glider} = 12.07$ (m/s) and $AoA = -3^\circ$. The pitching moment of the glider is determined as zero when AoA is selected as -3° . $C_m - \alpha$ graph shows that, mathematically, the design is stable if it has a negative gradient.

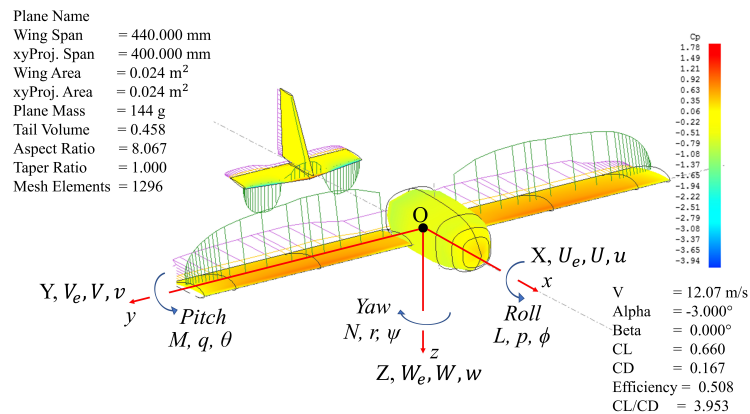


Figure 5. According to the Vortice Lattice Method (VLM), an analysis is done in the XFLR5[®] program. Accordingly, more C_L and lower C_D are calculated. The pressure points, which are more likely to be at the leading edge and less towards the tail, are shown by the right legend. In addition, axial and Euler parameters are represented on the glider.

Furthermore, it is crucial to determine the lift to drag C_L/C_D ratio since a higher C_L/C_D is typically one of the major goals in aircraft design. Here, C_L/C_D is calculated as 3.953. Accordingly, it has been observed that the glider can produce the lifting force greater than its own weight [30]. In Figure 6, lift to drag ratio with respect to AoA is presented. A Gaussian curve characteristic can be observed based on XFLR5 results, as expected. The AoA at the point where $\alpha = -3^\circ$ is taken since it gives the maximum ratio of L/D.

Aerodynamic coefficients match in both theoretical and simulation results. This is followed by the wing folding mechanism during separation of the glider from the container. Most folding theories are concerned with either speed of a stowed mechanism or its effect on the lift force. However, the strength of the wings and the folding mechanism should not be neglected. Deployment of the glider needs just a simple action from the user, since basic components are used, which are springs and magnets that are shown in Figure 7. In this figure, wing slots and magnets are represented in isometric view and springs can be seen in the top view of the glider. In our first configuration, only a spring is used in the wing folding mechanism.

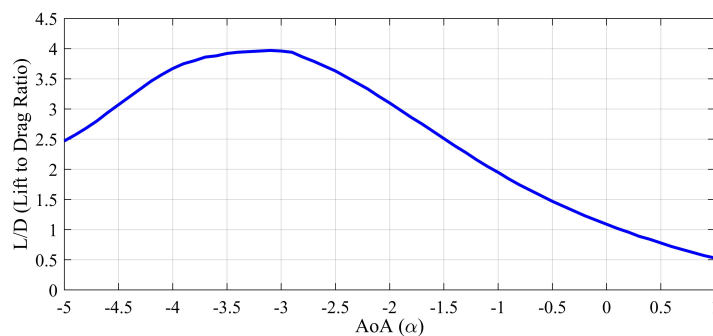


Figure 6. The $L/D - \alpha$ graph, which represents Gaussian curve, is acquired based on the 3D simulation that is given in Figure 5. AoA distribution only takes the maximum value at a certain angle interval. Therefore, in the remaining region except about $\alpha = -3^\circ$, there are exponential curve characteristics.

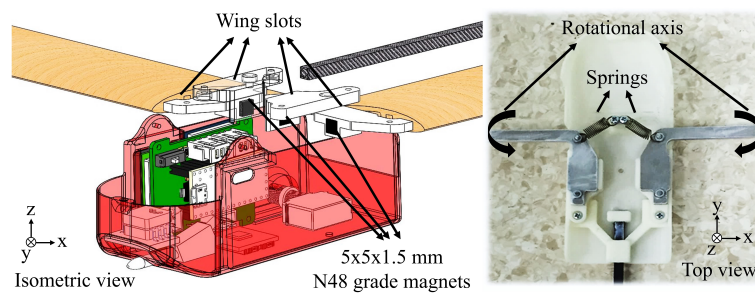


Figure 7. Left: the picture of the model shows magnets and dimensions and their positions on the wing slots; right: the picture of the folding mechanism including springs and rotational axis.

Folding mechanism and glider sizes are affected by the miniaturization of core technologies. However, the endurance of miniature drones' wings are questionable when they are exposed to maximum force [7–9]. The aim is to show that the wings are completely foldable even in unsuitable conditions. First, only a spring is used in the wing folding mechanism. This allows the mechanism to store potential energy. It would be desirable for the wing to be deployed parallel to the normal line, but the energy stored in the spring mechanism is designed to move the wing 8° forwards in 114 ms in Figure 8. However, after this movement of the wing, the wing moves back and falls short of the parallel wing position by 19° in 157 ms in an oscillating manner. When only a spring is used, it shows that the energy stored in the springs during the folding of the wings can not absorb the potential energy efficiently. For this reason, it was observed that the folding response of the wings has oscillations during their deployment and it is reported with the duration and angle.

The recoil of 19° has to be damped with additional equipment on the glider. To find the damping force needed, spring coefficient, k , should be determined first to evaluate repulsive force. K can be obtained experimentally by measuring ten fixed different weights whose mass are determined with three decimal precision scales with 1 mg resolution. Experimental results of k are detailed in Section 4. After that, neodymium magnets are used as a damping element and detailed in Section 4 in the second configuration. All equipment is designed to be used to simulate flight trajectory in MATLAB SIMULINK[®] by using equations that are mentioned in the mathematical modeling section. After finding all the necessary parameters and calculation results, the glider's components' mass can be expressed in Table 4.

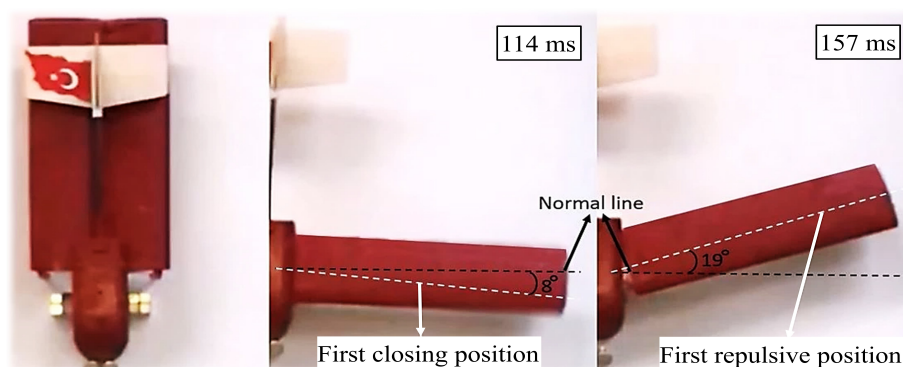


Figure 8. Left: picture of glider in folded position; middle: picture of the first deployed position exceedance with 8° in 114 ms; right: picture of first recoil, falling short with 19° in 157 ms.

Table 4. Mass properties of the glider's parts.

Payload	Unit Mass	Quantity
Fuselage, Lid	23.28, 13.00 (± 0.1)	1
T-Slot	1.70 (± 0.1)	2
L-Bracket	2.80 (± 0.1)	2
Screw & Nuts	0.40 (± 0.1)	5
Servo Motor, Holder, Horn	4.50, 1.10, 0.75 (± 0.1)	1
Main Wing	7.31 (± 0.1)	2
Tail Wings	3.65 (± 0.1)	1
Fiber Rod	1.01 (± 0.1)	2
Magnets	0.29 (± 0.1)	4
Camera	2.50 (± 0.1)	1
9V Battery	34.00 (± 0.1)	1
Electronics	22.80 (± 1)	1
Pitot Tube	2.50 (± 0.1)	1
Pressure Sensor	7.00 (± 0.1)	1
SUM	143.89 (± 4.5) g	

The system model could be done by designing the equipment the same as the results, including their mass. Glider force and moment stability could be achieved during 12 (m/s) flight speed and $\alpha = -3^\circ$. According to obtained speed and x , y , and z positions of the glider, and the glide duration can be calculated. Glide duration and helical path can be controlled by two different control inputs that are elevator and rudder. The elevator, which is the aerodynamic control for pitch angle, can also affect efficient lift and AoA. It is positioned at the rear of the stabilizer that is attached to the fixed sections by hinges. Because the elevator can move, it varies the amount of force generated by the tail surface. The elevators work by changing the effective shape of the airfoil of the horizontal stabilizer. A helical path with a diameter of 85.03 m maximum could be maintained for 118.3 s until completion when the elevator -8.5° and rudder 0.5° under axial wind disturbances. Atmospheric conditions and wind properties must be modeled due to the glider not being released in a controlled test environment. The wind pattern is set to be about 1.5 m/s for each axis. Wind speeds are denoted as u , v and w , which are representing noise, and shown in the same axis set in Figure 9. In this way, the glider is subjected to a more realistic test and the results are more accurate.

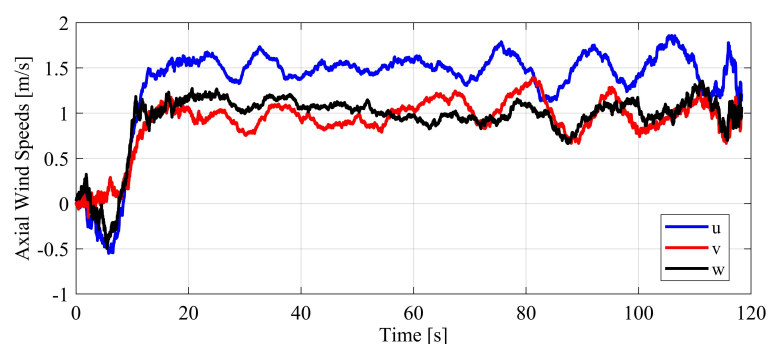


Figure 9. The wind profiles applied during the descent of the glider are shown. It will follow a helical path under wind disturbances. To have more realistic simulation, a wind profile with an approximate 1.5 m/s amplitude was applied for u , v and w -axes.

Under wind disturbances, a flight path can also be seen in Figure 10. During descent, a 1.5 cycle, whose diameter is bigger than other helical cycles, could be seen at the beginning of the path due to the glider not reaching the speed limit, which is needed for the stability. However, when the glider is about 310 m in height, equal helices are seen since the limit speed is reached. Moreover, the glider is separated from a container with initial speed 0 (m/s).

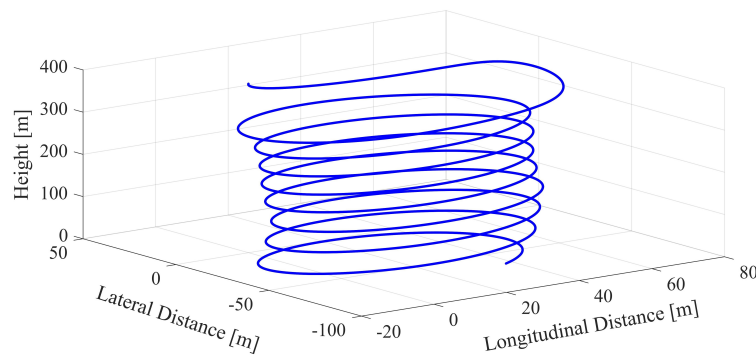


Figure 10. Helical path is followed by glider that shows a stable flight during descent.

The graph of the helical path diameter derived from longitudinal distance and lateral distance with respect to time shows that the time required for stable flight is 23.7 s. As a result, the glider should be stable at about 310 m at 23.7 s. According to analysis and simulations in this section, it is shown that the wing-folding structure is safe and that the glider can fly and hover according to the rules.

4. Experimental Work

In this section, the effects of the magnets that are used for the wing-folding mechanism and their damping effect, the strength of the wings and the wing slots, where the magnets are attached, along with the actual flight test are included.

4.1. Magnet Effects

First of all, the potential energy stored must be found in the spring by calculating the spring coefficient, k . Then, the appropriate magnet sizes can be determined by calculating the forces depending on the angles that can be seen in the first wing-folding configuration, which is the only spring that is used. Ten different experiments are done to determine k by using the experimental data and curve fitting plot is also given with %1.42 error in Figure 11 [31]. In this figure, k is obtained by measuring the spring extension according to ten different weights on the same spring. A precision balance (TRYTE TECHNOLOGY WB3003N, Hunan, China) is used for weight measurement. The difference between the initial and ending positions of the spring was recorded with an optical microscope (Olympus SZX-7, Olympus Corporation, Tokyo, Japan and PointGrey GS3-U3, FLIR Integrated Imaging Solutions Inc., Richmond, BC, Canada). According to the obtained results, the points are combined with the error of 1.42%, so that k can be calculated by the slope of the plot.

By using the curve fitting method, the equation of this plot could be derived as $150.9x + 0.2$ by MATLAB[®] and k is calculated as $k = 150.9$ (N/m). Repulsive force, F_{rep} , can be determined $F_{rep} = 0.6941$ (N) when the elongation of the spring is $\delta_x = 4.6$ mm for 19° wing angle. F_{rep} is the maximum force that has to be damped by the folding mechanism with additional neodymium magnets. The attraction forces of these magnets, which will be used to absorb the potential energy and repulsive forces generated during the folding of the wing, should be calculated. This force must be greater than the forces that oscillate the wing during folding. Magnetic attraction force of two block magnets can be seen in Figure 12. In this figure, the magnetic flux is the net number of field lines that are passing through that surface. Because the magnets are conjoined, the flux density could be seen more in the corner regions.

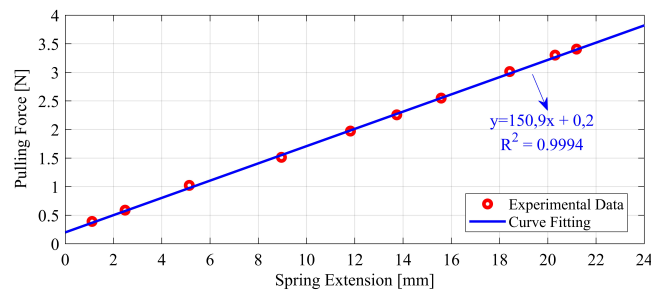


Figure 11. Experimental results (red dots) of k shows, coefficient of spring with respect to measure masses that are known. Curve fitting (blue line) method k is obtained as an equation to determine average k .

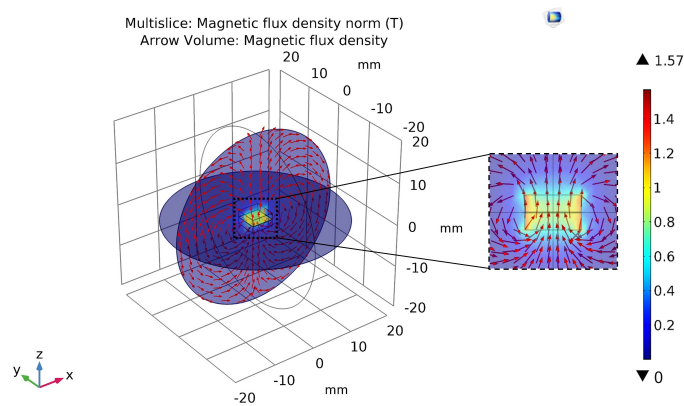


Figure 12. Two block type magnets, which are acting as a damping element; analysis can be seen. The aim is to determine magnetic attraction force by a COMSOL[®] Magnetic Fields Module.

The attraction force between these magnets varies depending on the distance δ_z , which is between 0 mm and 10 mm. Depending on the distance between the magnets, the magnetic attraction force also decreases. According to the parametric analysis, the force calculation is done when the step size is 0.01 mm. The attraction force graph of magnets can be seen in Figure 13. In this figure, the graph shows that the force is affected by the distance between magnets as an exponential function as expected. Such a consequence is due to the nature of nonlinear behavior in the magnetic field. For this reason, it is very difficult to separate the magnets when they are attached to each other.

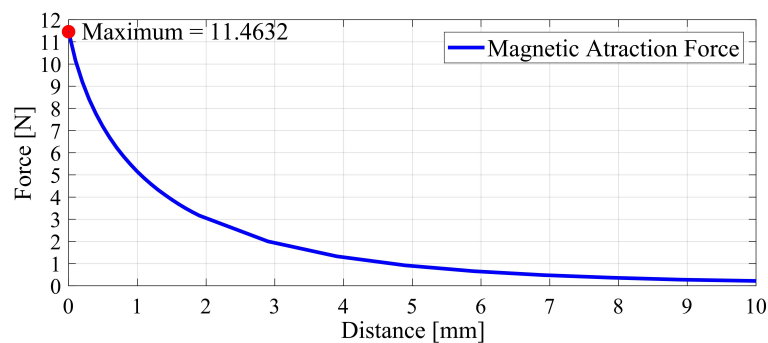


Figure 13. Magnetic force calculation is obtained by COMSOL[®] in AC/DC Module. Two neodymium magnets (N48 grade) are positioned in the same center line and parametric analysis is performed. Depending on the distance between the magnets, an exponential force curve is obtained as expected.

The maximum magnetic force is calculated as 11.46 N when the magnets are attached. When the wings become parallel to the glider's body after separating from the container, the magnets will also become parallel and attached. In this case, it is necessary to apply the force, which should be greater than maximum magnetic force, in order to have oscillation wings. However, $F_m = 11.46$ N is almost 15 times greater than the repulsive force F_{rep} ; thus, it is guaranteed that wings can be deployed without repulsive force and oscillation. After the addition of the magnets to the first configuration, the effect of the wing-folding duration and the oscillation is also investigated. The completed wing-folding mechanism's results, including magnets and springs, are given in Figure 14. In this figure, it seems that the wings are folded without any oscillation and are much faster than just using the spring.

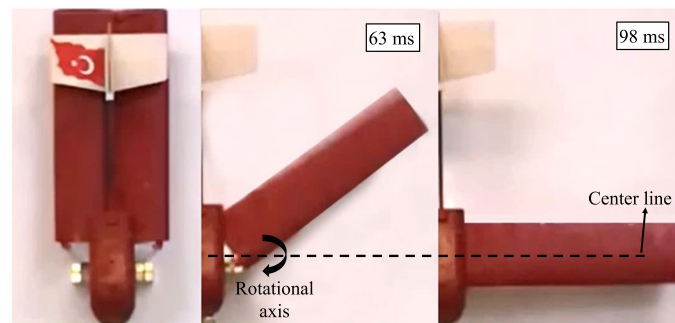


Figure 14. Wings are deployed in 98 ms. left: picture of instant position; middle: during the deployment; right: picture of the completed deployment of the wings.

Another reason for the faster folding of the wings is that when the magnets are affected at the same magnetic field range in their work space, it increases the folding speed. Based on this, it is shown that the wings are supposed to fold faster and without any overshoot as expected.

4.2. Safety of Folding Mechanism

As the final step in the folding mechanism, the strength of the mechanism when the glider is hovering should be determined. To make (1°) circular motion on the wings, spring should be elongated by $\delta_x = 1.7452$ mm. Spring force, F_s , is calculated as $F_s = 0.263$ N. All the forces that are acting on the glider could be examined in two parts, which are the gravitational force of the wings, F_G , and the drag forces, F_D . For a 144 g glider, maximum F_G could be obtained when the critical angle of attack is reached or exceeded. $F_D = 0.383$ N, $F_G = 0.071$ N and $F_m = 11.46$ N can be used to calculate total maximum force that is acting on the glider's wing slot. Because the wing-folding system can not oscillate due to the magnets, by taking F_m as the maximum testing force, fatigue of the wing-folding mechanism can be calculated. Tensile strength of the Acrylonitrile butadiene styrene (ABS) plastic, which is used in wing's slot section, is 42.5 MPa and the balsa wood tensile strength, which is used in the wing, is also 7.6 MPa. Accordingly, it should be checked whether these materials are safe or not according to result from COMSOL[®] analysis. Calculated maximum test force acting on the glider is determined as $F_m = F_t = 11.46$ N, which applies to both the slot and wing sections. First, slot part analysis under this force could be seen in Figure 15. In this figure, 11.46 N is applied as an impulse signal from the wing slots, where the magnets are located, to the center of the magnet. As expected, this part is fixed to the glider body on the z-axis so that the tensile strength is seen on the same surface with the magnets. Possible deformations in this region will prevent the wings from aligning themselves in a parallel position after opening. Therefore, it appears that only a deflection of $4.308 \mu\text{m}$ appears in the wings for the maximum test force.

Since tensile stress of ABS is almost 50 times greater than obtained 0.82 MPa, the design and the components are safe to be used. Furthermore, ABS slot could be cracked only if 87.92 (N) is applied; however, this force is not exceeded in the design. As a second part of the safety test, the wing is analyzed under the same test force and this analysis can be seen in Figure 16. In this figure, the wing profile is strengthened by applying epoxy on the surface with approximately 100 μm thickness. The structure shows a highly strengthened profile. Stress can be seen more on the trailing edge corner and l-bracket part on the wing connection. Due to the l-bracket having a length of 20 mm, it (shown in Section 3, Figure 7 rotational axis) is not attached to whole wing structure, which is 200 mm. Thus, stress can be seen more on the leading and trailing edge corners where the l-bracket is attached to the wing.

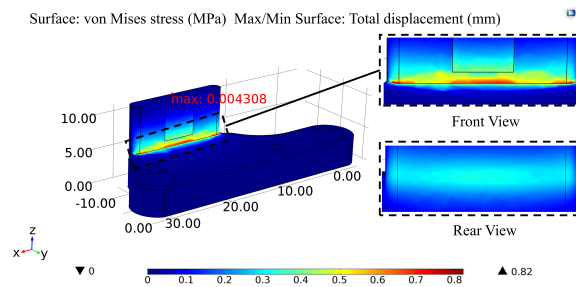


Figure 15. Shows the stress of the slots as a result of the impact on the wing-folding mechanism. Maximum deflection is obtained 4.308 μm on the slot’s top edge. The maximum stress point 0.82 MPa is seen at the center point of the front view; 0.3–0.35 MPa stress could also be seen in the rear view in magnified scales.

The force required to detach an l-bracket from its wing connection point is determined as 97.32 (N) by COMSOL® analysis. These results show that the chosen wing-folding mechanism is totally safe and reliable. Finally, the wings are deployed by releasing the folding position 25 times in succession for both configurations. During this test, wing motion is recorded on a 240 fps camera (Yi 4K, Shanghai Xiao Yi Technology Co. Ltd, shanghai, China). For the first configuration with only a spring, the first closing position time (1); the first oscillation movement position time (2); and complete closure time (3) along with only the full closure time (4) for the second configuration with magnets are shown in Figure 17.

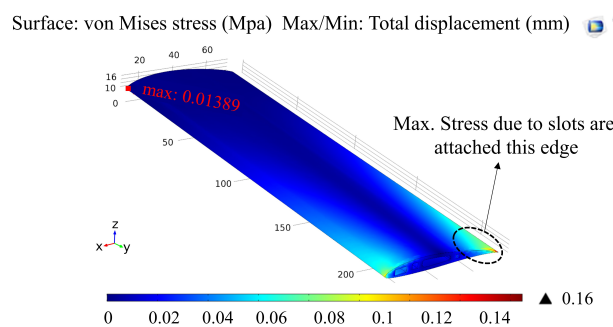


Figure 16. Maximum deflection is obtained 13.89 μm on the wing’s corner edge. Maximum stress point 0.16 MPa is seen as the same as wing slots. Since the wings are indirectly influenced by the test force during deployment, there is not as much tension as the wing slots.

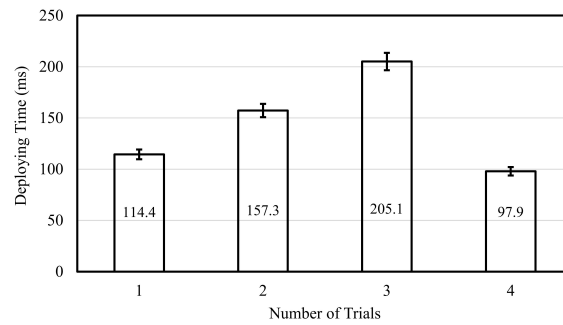


Figure 17. Two configurations of the wing-folding mechanisms’ deployment durations are shown. The wing exceeds the perpendicular axis to the glider by 8° and the oscillation starts (1), the wing closes by 27° due to oscillation and starts opening again (2) and then there is complete closure time (3). The figure shows that with magnets (4), the wing-folding mechanism can be deployed two times faster without any overshoot.

4.3. Flight Data

In this section, a flight test of glider, which was designed according to the competition rules and proved to perform tasks with the simulation results on MATLAB/Simulink[®], is given. The glider, which is launched with the rocket in the race, is separated autonomously from the rocket at a height of 600 m. Experiments have been conducted with the drone mechanism (DJI S1000 PLUS, Shenzhen Dajiang Baiwang Technology Co., Ltd., shenzhen, China), which can reach 400 m in height. The glider left the container at 400 m and could glide until landing. It is possible to collect data such as glider speed, altitude, temperature and pressure of the flight through the ground station. After separation, the glider has followed a helical orbit. The duration of the descent varied between approximately 115–122 s for different tests. According to the competition rules, the gliders are expected to fly as close to 120 s as possible. A time difference of about maximum 4% has been calculated and good results have been obtained for a system without active control. The tests followed a flight trajectory with a characteristic as in Figure 10. Similarly, although it had a wider orbital diameter in the first 1.5–2 turn, it became stable after 25–30 s and was able to draw co-helical circles. Similar to the longitudinal and lateral distances, an orbital diameter of 63 m minimum and 119 m maximum was observed. The glider, which has to hover at a diameter of up to 1000 m, has successfully carried out the phugoid motion as expected and has maintained the diameter within the desired limits. Figure 18 shows the successful flight trajectories performed in the tests.

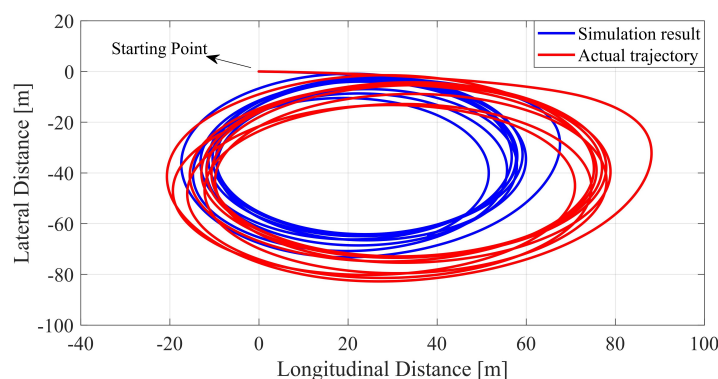


Figure 18. In the meantime, during the tests, the orbits of the glider are visible. The orbits are built with a GPS unit. The starting points and trajectory of the orbit are indicated by the arrow. The glider, starting from the starting point, which is shown in the figure with an arrow, made the descent by drawing co-helical circles. In addition, 398.15 m wide and 117.1 s long successful flight orbits are shown when the wind speed is about 2 m/s.

5. Discussion

In this study, a foldable mini-glider design and implementation was described in detail while design constraints were defined based on CanSat competition rules. By mentioning the materials used in the design and the selection criteria, the glider's mathematical model and system dynamics are presented. Flight limitations were also presented according to aerodynamic analyses, supported by design simulation results. A new method has been done and reported for more optimized operation by testing the wing deploying and folding times. Tests have been made for the reliability of the wing-folding mechanism, and a safe and easy to implement design has been done. Finally, experimental flight results were also reported to show a good match with theoretical results. Since the proposed glider has a passive flight structure and limited sensor capability due to regulations of CanSat Competition, the simulation parameters were verified by using actual experimental results via required path-following in the desired circular diameter and flight time.

Accordingly, as a contribution to the literature, an unmanned glider designed under certain rules and constraints is described. It has been shown what should be considered in a lightweight and foldable design of a glider. The lightweight glider was designed to have a higher C_L and a lower C_D coefficient than similar studies. According to similar studies of the same size, there was no problem in transmitting data from the sensors even when it is inside of the rocket, in the container or outside the container. The wing-folding of the glider was realized by a completely passive-autonomous mechanical mechanism and fulfilled the desired objectives without any initial condition at low altitude. The designed glider can receive telemetry data and also allows flight information to be sent to the ground station. With its lightweight design and low power consumption, the glider can obtain relevant flight data from all sensors. Thus, aerodynamically, a more successful design has been made.

In the experiments, the wings were opened successfully when glider separation from the container. If there is a delay or failure during wing deployment, the glider would not be able to fly in co-helical orbits and land. For this reason, a specialized wing-folding mechanism was presented. Simple equipments (springs-magnets) were utilized based on offered mechanism. It was also seen that it gave faster opening results compared to similar designs of the same size of folding mechanism. The deployment speed of the wings was tested with repetitive experiments (25 times) for the two different wing-folding configurations. Deployment duration was recorded by high speed camera and the strength of the mechanism was also reported.

The oscillation caused by the momentum generated during the opening and closing of the wings has also been examined. The results were shown by the analysis, and the experimental setups in which a mechanism with fast and reliable opening of the wings were obtained. Lastly, more stable flight is shown in experimental studies than in similar examples of glider without any motor and active controller. It has been observed that a successful phugoid motion has been captured. In this mode, a continuously descending flight orbit was observed. The glider system successfully opened its wings when it left the container, just like in the test results, and successfully completed the competition goals.

Author Contributions: Throughout the project, A.A.D. was responsible for the implementation of the glider, experiments, COMSOL[®] analysis, and mathematical models. H.U. completed all manufacturing processes of the related model and ground-station interface. He was also responsible for the development of the wing-folding principles.

Conflicts of Interest: The authors declare no conflict of interest.

Abbreviations

The following abbreviations are used in this manuscript:

ABS	Acrylonitrile Butadiene Styrene
AoA	Angle of Attack
MAC	Mean Aerodynamic Chord
NACA	National Advisory Committee for Aeronautics
PID	Proportional-Integral-Derivative
SD	Secure Digital
VLM	Vortice Lattice Method

References

1. Truszkowski, W.; Hinchey, M.; Rash, J.; Rouff, C. NASA's swarm missions: The challenge of building autonomous software. *IT Prof.* **2004**, *6*, 47–52. [[CrossRef](#)]
2. Dai, Y.S.; Levitin, G. Reliability and Performance of Tree-structured Grid Services. *IEEE Trans. Reliab.* **2006**, *55*, 337–349. [[CrossRef](#)]
3. Tang, E.Z.S.; Hii, J.D.S.; Liew, R.W.; Tang, D.J.W.; Tan, J.W.K. *SwitchBlade*; The Singapore Public Service: Singapore, 2014.
4. Kessler, S.; Spearing, S.; Kirkos, G. Design of a high-g unmanned aerial vehicle structure. In Proceedings of the 2000 World Aviation Conference, San Diego, CA, USA, 10–12 October 2000.
5. Lyon, D.H. A military perspective on small unmanned aerial vehicles. *IEEE Instrum. Meas. Mag.* **2004**, *7*, 27–31. [[CrossRef](#)]
6. Smith, T.; McCoy, E.; Krasinski, M.; Limaye, S.; Shook, L.; Uhelsky, F.; Graham, W. Ballute and parachute decelerators for FASM/QUICKLOOK UAV. In Proceedings of the 17th AIAA Aerodynamic Decelerator Systems Technology Conference and Seminar, Monterey, CA, USA, 19–22 May 2003.
7. Dufour, L.; Owen, K.; Mintchev, S.; Floreano, D. A Drone with Insect-Inspired Folding Wings. In Proceedings of the 2016 IEEE/RSJ International Conference on Intelligent Robots and Systems, Daejeon, Korea, 9–14 October 2016.
8. Smith, A.J. Aerial Deployed Unfolding Autonomous Glider System. In Proceedings of the 53rd AIAA Aerospace Sciences Meeting, Kissimmee, FL, USA, 5–9 January 2015.
9. Mintchev, S.; Daler, L.; L'Eplattenier, G.; Saint-Raymond, L.; Floreano, D. Foldable and self-deployable pocket sized quadrotor. In Proceedings of the 2015 IEEE International Conference on Robotics and Automation (ICRA), Seattle, WA, USA, 26–30 May 2015; pp. 2190–2195.
10. Andrews, S.; Grossman-Ponemon, B.; Hendricks, S.M.; Hong, G.; McKenzie, C.; Morette, K. *Design of a Micro-Class Aircraft for the SAE AeroEast Heavy Lift Competition 2012*; Worcester Polytechnic Institute: Worcester, MA, USA, 2012.
11. Chauffaut, C.; Escareno, J.; Lozano, R. The transition phase of a gun-launched micro air vehicle. *J. Intell. Robot. Syst.* **2013**, *70*, 119–131. [[CrossRef](#)]
12. Landon, S.D. Development of Deployable Wings for Small Unmanned Aerial Vehicles Using Compliant Mechanisms. Master's Thesis, Brigham Young University, Provo, UT, USA, 2007.
13. Koehl, A.; Rafaralahy, H.; Boutayeb, M.; Martinez, B. Aerodynamic modelling and experimental identification of a coaxial-rotor UAV. *J. Intell. Robot. Syst.* **2012**, *68*, 53–68. [[CrossRef](#)]
14. Felton, S.; Tolley, M.; Demaine, E.; Rus, D.; Wood, R. A method for building self-folding machines. *Science* **2014**, *345*, 644–646. [[CrossRef](#)] [[PubMed](#)]
15. Available online: <http://www.cansatcompetition.com> (accessed on 1 June 2015).
16. Wu, H.Y.; Sun, D.; Zhou, Z.Y.; Xiong, S.S.; Wang, X.H. Micro air vehicle: Architecture and implementation. In Proceedings of the IEEE International Conference on Robotics Automation, Taipei, Taiwan, 14–19 September 2003; pp. 534–539.
17. Lissaman, P.B.S. Low-Reynolds-number airfoils. *Annu. Rev. Fluid Mech.* **1983**, *15*, 223–239. [[CrossRef](#)]
18. Navy, U.S. *Sonobuoy Tube-Launched UAV*; SBIR.gov: El Cerrito, CA, USA, 2004.

19. Gao, R.S.; Elkins, J.W.; Frost, G.J.; McComiskey, A.C.; Moore, F.L.; Murphy, D.M.; Ogren, J.A.; Petropavlovskikh, I.; Rosenlof, K.H. A Novel Approach to Atmospheric Measurements Using Gliding UASs. In *Dynamic Data-Driven Environmental Systems Science*; Springer: Cham, Switzerland, 2015; pp. 10–15.
20. Kräuchi, A.; Philipona, R. Return glider radiosonde for in situ upper-air research measurements. *Atmos. Meas. Tech.* **2016**, *9*, 2535–2544. [[CrossRef](#)]
21. Cai, G.; Dias, J.; Seneviratne, L. A survey of small-scale unmanned aerial vehicles: Recent advances and future development trends. *Unmanned Syst.* **2014**, *2*, 175–199. [[CrossRef](#)]
22. Roberts, L.J.; Bruck, H.A.; Gupta, S.K. Modeling of Dive Maneuvers for Executing Autonomous Dives with a Flapping Wing Air Vehicle. *J. Mech. Robot.* **2017**, *9*, 061010. [[CrossRef](#)]
23. Trautz, M.; Kunstler, A. Deployable folded plate structures-folding patterns based on 4-fold-mechanism using stiff plates. In *Symposium of the International Association for Shell and Spatial Structures (50th. 2009. Valencia). Evolution and Trends in Design, Analysis and Construction of Shell and Spatial Structures: Proceedings*; Editorial Universitat Politècnica de València: Valencia, Spain, 2010.
24. Beeler, S.C.; Moerder, D.D.; Cox, D.E. *A Flight Dynamics Model for a Small Glider in Ambient Winds*; NASA Technical Reports Server: Washington, DC, USA, 2003.
25. Bachuta, M.J.; Czyba, R.; Janusz, W.; Yurkevich, V.D. UAV glider control system based on dynamic contraction method. In *Proceedings of the 2012 17th International Conference on Methods and Models in Automation and Robotics (MMAR)*, Miedzyzdroje, Poland, 27–30 August 2012.
26. Yechout, T.R. *Introduction to Aircraft Flight Mechanics*; The American Institute of Aeronautics and Astronautics: Reston, VA, USA, 2003.
27. Garza, F.R.; Morelli, E.A. *A Collection of Nonlinear Aircraft Simulations in Matlab*; NASA Technical Reports Server: Washington, DC, USA, 2003.
28. Etkin, B.; Reid, L.D. *Dynamics of Flight: Stability and Control*; Wiley: New York, NY, USA, 1996; Volume 3.
29. Dilão, R.; Fonseca, J. Dynamic trajectory control of gliders. In *Advances in Aerospace Guidance, Navigation and Control*; Springer: Berlin/Heidelberg, Germany, 2013; pp. 373–386.
30. Mueller, T.J. *Fixed and Flapping Wing Aerodynamics for Micro Air Vehicle Applications*; American Institute of Aeronautics and Astronautics: Reston, VA, USA, 2001; Volume 195.
31. Lancaster, P.; Salkauskas, K. *Curve and Surface Fitting: An Introduction*; Academic Press: London, UK, 1986.



© 2018 by the authors. Licensee MDPI, Basel, Switzerland. This article is an open access article distributed under the terms and conditions of the Creative Commons Attribution (CC BY) license (<http://creativecommons.org/licenses/by/4.0/>).